

# Solar neutrinos: the SNO salt phase results and physics of conversion

P. C. de Holanda<sup>1</sup> and A. Yu. Smirnov<sup>2,3</sup>

- (1) Instituto de Física Gleb Wataghin – UNICAMP, 13083-970 Campinas SP, Brasil
- (2) The Abdus Salam International Centre for Theoretical Physics, I-34100 Trieste, Italy
- (3) Institute for Nuclear Research of Russian Academy of Sciences, Moscow 117312, Russia

## Abstract

We have performed analysis of the solar neutrino data including results from the SNO salt phase as well as the combined analysis of the solar and the KamLAND results. The best fit values of neutrino parameters are  $m^2 = 7.1 \cdot 10^{-5} \text{ eV}^2$ ,  $\tan^2 \theta = 0.40$  with the boron flux  $\Phi_B = 1.04$ . New SNO results strongly disfavor maximal mixing and the h-LMA region ( $m^2 > 10^{-4} \text{ eV}^2$ ) which is accepted now at the 3 level. We find the 3 upper bounds:  $m^2 < 1.7 \cdot 10^{-4} \text{ eV}^2$  and  $\tan^2 \theta < 0.64$ , and the lower bound  $m^2 > 4.8 \cdot 10^{-5} \text{ eV}^2$ . Non-zero  $\theta_{13}$  mixing does not change these results significantly. The present data determine quantitatively the physical picture of the solar neutrino conversion. At high energies relevant for SNO and Super-Kamiokande the deviation of the effective survival probability from the non-oscillatory value is about 10–14%. The oscillation effect contribution to this difference is about 10% and the Earth regeneration about 3–4%. At low energies ( $E < 1 \text{ MeV}$ ) the matter corrections to vacuum oscillation effect are below 5%. The predictions for the forthcoming measurements are given which include the spectral distortion and CC/NC ratio at SNO, the Day-Night asymmetry, the KamLAND spectrum and rate.

# 1 Introduction

The SNO –II (salt phase) results [1] have further confirmed correctness of both the neutrino fluxes predicted by the Standard Solar Model (SSM) [2] and picture of the solar neutrino conversion based on the MSW effect [3, 4]. Together with the results from the SNO phase-I [5], Homestake [6], SAGE [7], GALLEX [8], GNO [9] and Super-Kamiokande [10, 11] experiments as well as from the reactor experiment KamLAND [12] the latest SNO results lead to better determination of the oscillation parameters. This improvement allows one to make two important qualitative statements [1]:

the h-LMA region, which corresponds to  $m^2 > 10^{-4} \text{ eV}^2$ , is strongly disfavored (being accepted at the 3 level);

there is a substantial deviation of 1-2 mixing from the maximal one, and the latter is rejected by more than 5 standard deviations.

These statements have been confirmed by followed analyzes [13, 14, 15, 16, 17, 18].

There are two key points of the SNO –II publication: (i) new measurement of the total active Boron neutrino flux with enhanced neutral current sensitivity, and (ii) data analysis without assumption of the undistorted neutrino spectrum. They lead to larger (than pre-salt) value of the neutrino flux measured by the neutral current (NC) reaction and smaller flux measured by the charged current (CC) reaction [1]. As a result, the ratio of neutrino fluxes [1]:

$$\frac{CC}{NC} = 0.306 \pm 0.026(\text{stat}) \pm 0.024(\text{syst}) \quad (1)$$

turns out to be smaller than the value from pre-salt measurements:  $0.346 \pm 0.048 = 0.046$  [5]. It is, however, larger than the value which corresponds to the NC flux determined previously without constraint of the undistorted spectrum:  $CC/NC = 0.274 \pm 0.073$  [5].

The ratio (1) is also smaller than the expected one. In the previous paper [19] we have predicted that the central value of the ratio (which corresponds to the best fit point) and the 3 error bars equal:  $CC/NC = 0.33 \pm 0.15 = 0.07$ . It was pointed out that values  $CC/NC < 0.35$  exclude the h-LMA region. Furthermore, precise measurements of  $CC/NC$  should strengthen the upper bounds on mixing and  $m^2$  [19].

Confronting the prediction for  $CC/NC$  with the experimental result (1) one can understand consequences of (1) immediately. According to fig.10 of ref. [19] (where we show the contours of constant  $CC/NC$  ratio in the  $m^2 - \tan^2$  plot) the ratio  $CC/NC$  decreases with  $m^2$  and  $\tan^2$ . Therefore, with the SNO salt results the best fit point and the allowed region shift toward the smaller values of  $m^2$  and  $\tan^2$ . Maximal mixing and the h-LMA region should be further disfavored. This is indeed confirmed by the detailed studies [1].

In this paper we present our analysis of the solar neutrino data including the SNO –II fluxes (sec. 2). We perform a combined analysis of the solar neutrino and KamLAND

results (sec. 3). Possible effect of 1-3 mixing is considered in sec. 4. We show that after the SNO-II measurements, physics of the solar neutrino conversion is essentially determined. In particular, relative contributions of the adiabatic conversion in matter and the oscillation effect for different energies can be quantified (sec. 5). In sec. 6 the expected spectrum distortion at SNO is studied. In sec. 7 we give predictions for the future experiments. The conclusions are presented in sec. 8.

## 2 Solar Neutrinos with the SNO salt-phase results

In the analysis we use the following data set:

3 total rates: (i) the Ar-production rate,  $Q_{Ar}$ , from Homestake [6], (ii) the Ge production rate,  $Q_{Ge}$ , from SAGE [7] and (iii) the combined Ge production rate from GALLEX [8] and GNO [9];

44 data points from the zenith-spectra measured by Super-Kamiokande during 1496 days of operation [10, 11];

34 day-night spectral points from SNO [5];

3 fluxes from the SNO salt phase [1] measured by the CC-, NC and ES-reactions. We treat correlations of these fluxes following prescription in [20].

Altogether the solar neutrino experiments provide us with 84 data points.

All the solar neutrino fluxes, but the boron neutrino flux, are taken according to SSM BP2000 [2]. The boron neutrino flux measured in the units of the Standard Solar Model flux [2],  $f_B = F_B / F_B^{SSM}$ , is treated as a free parameter (here  $F_B^{SSM} = 5.05 \cdot 10^{10} \text{ cm}^{-2} \text{ s}^{-1}$ ). For the hep neutrino flux we take fixed value  $F_{hep} = 9.3 \cdot 10^8 \text{ cm}^{-2} \text{ s}^{-1}$  [2, 21].

We use the same procedure of analysis as in our previous publication [22, 19]. In analysis of the solar neutrino data as well as in the combined analysis of the solar and KamLAND results we have three fit parameters:  $m^2$ ,  $\tan^2 \theta$  and  $f_B$ .

We perform the  $\chi^2$  test defining

$$\chi_{\text{sun}}^2 = \chi_{\text{rate}}^2 + \chi_{\text{SK}}^2 + \chi_{\text{SNO-I}}^2 + \chi_{\text{SNO-II}}^2; \quad (2)$$

where  $\chi_{\text{rate}}^2$ ,  $\chi_{\text{SK}}^2$ ,  $\chi_{\text{SNO-I}}^2$  and  $\chi_{\text{SNO-II}}^2$  are the contributions from the total rates, the Super-Kamiokande zenith spectra, the SNO day and night spectra and the SNO fluxes from the salt phase correspondingly. The number of degrees of freedom is  $84 - 3 = 81$ .

The minimum,  $\chi_{\text{sun}}^2(\text{min}) = \text{dof} = 67 = 81$  is achieved at

$$m^2 = 6.31 \cdot 10^5 \text{ eV}^2; \quad \tan^2 \theta = 0.39; \quad f_B = 1.063; \quad (3)$$

From the pre-salt analysis we had:  $(m^2; \tan^2) = (6.15 \pm 1.6; 0.41) [22]$ . So, the SNO-II data only slightly shifted the best fit point to smaller values of  $m^2$  and  $\tan^2$ . The boron neutrino flux was smaller:  $f_B = 1.05$ .

We construct the contours of constant confidence level in the  $m^2 - \tan^2$  plot (g.1) using the following procedure. We perform minimization of  $\chi^2$  with respect to  $f_B$  for each point of the oscillation plane, thus getting  $\chi^2_{\text{sun}}(m^2; \tan^2)$ . Then the contours are defined by the condition  $\chi^2(m^2; \tan^2) = \chi^2(\text{min}) + \Delta^2$ , where  $\Delta^2 = 2.3; 4.61; 5.99; 9.21$  and  $11.83$  are taken for 1, 90%, 95% and 99% C.L. and 3.

In contrast to the best fit point, the influence of the SNO-II data on the size of allowed region, especially for high confidence levels is much stronger. The data reduce substantially the allowed region from the parts of large  $m^2$  and  $\tan^2$ . The borders of 3 region are shifted as  $(4.5 \pm 1.6) \cdot 10^4 \text{ eV}^2$  for  $m^2$ , and  $(0.84 \pm 0.64)$  for  $\tan^2$ .

Shift of the 1 contour is much weaker. Projecting the 1 region from g.1 we find the intervals:

$$m^2 = (3.8 \pm 1.0) \cdot 10^5 \text{ eV}^2; \quad \tan^2 = 0.325 \pm 0.475: \quad (4)$$

The lower bounds for  $m^2$  and  $\tan^2$  are practically unchanged.

### 3 Solar neutrinos and KamLAND

The KamLAND data have been analyzed using the Poisson statistics. Minimizing

$$\chi^2_{\text{KL}} = \sum_{i=1,13}^X \left[ 2 N_i^{\text{th}} - N_i^{\text{obs}} + N_i^{\text{obs}} \ln \frac{N_i^{\text{obs}}}{N_i^{\text{th}}} \right] \quad (5)$$

we find the best fit point

$$m^2 = 7.24 \cdot 10^5 \text{ eV}^2; \quad \tan^2 = 0.52: \quad (6)$$

Confronting the oscillation parameters determined independently from the solar neutrino experiments (3) and KamLAND (6) one can check CPT and search for new physics \beyond LMA". Since there is no significant change in the best fit point and 1 region for solar neutrinos, status of the CPT check is practically unchanged in comparison with the pre-salt analysis. The data are well consistent with the CPT conservation. As before, there is an overlap of the 1 regions of oscillation parameters found from the solar data and KamLAND results. The b.f. point (3) is at the border of 95% C.L. region allowed by KamLAND [12].

Assuming CPT conservation we have performed a combined fit of the solar neutrino data and KamLAND spectral results. We calculate the global  $\chi^2$

$$\chi^2_{\text{global}} = \chi^2_{\text{sun}} + \chi^2_{\text{KL}}: \quad (7)$$

There are 84 (solar) + 13 (KamLAND) data points - 3 free parameters = 94 d.o.f.. The absolute minimum,  $\chi^2_{\text{global}}(\text{min}) = 73.4 = 94$  is at

$$m^2 = 7.13 \cdot 10^5 \text{ eV}^2; \quad \tan^2 \theta = 0.40; \quad f_B = 1.038: \quad (8)$$

The SNO salt results have shifted the best global  $\chi^2$  point to smaller  $m^2$  and  $\tan^2 \theta$  in comparison with the results of previous analysis [19]:  $m^2 = 7.30 \cdot 10^5 \text{ eV}^2$ ,  $\tan^2 \theta = 0.41$ ,  $f_B = 1.05$ .

We construct the contours of constant confidence level in the  $m^2$  -  $\tan^2 \theta$  plot (Fig. 2) using the same procedure as in sec. 2. According to Fig. 2 the intervals of parameters obtained by projection of the 1  $\sigma$  allowed region equal

$$m^2 = (6.4 \text{ -- } 8.4) \cdot 10^5 \text{ eV}^2; \quad \tan^2 \theta = 0.33 \text{ -- } 0.48: \quad (9)$$

Notice that inclusion of the KamLAND result does not change the 3  $\sigma$  upper bounds on  $m^2$  and  $\tan^2 \theta$  (compare with Fig. 1). However, KamLAND further strengthens the lower bound on  $m^2$ :

$$m^2 > 4.8 \cdot 10^5 \text{ eV}^2; \quad (3 \sigma): \quad (10)$$

As a result of the SNO-II measurements, the h-LMA region,  $m^2 (12 \text{ -- } 16) \cdot 10^5 \text{ eV}^2$ , is strongly disfavored being accepted with respect to the global minimum (8) at about 3 level only.

From Fig. 2 we get the following upper bounds on mixing:

$$\tan^2 \theta \begin{cases} \geq 0.48; & 1 \\ < \begin{cases} 0.55; & 2 \\ 0.64; & 3 \end{cases} \end{cases} \quad (11)$$

Maximal mixing is excluded at 5  $\sigma$ . These bounds follow from the solar neutrino data being practically unaffected by KamLAND.

To check stability of our results we have performed analysis taking the boron neutrino flux as it is predicted by the SSM:  $f_B = 1$ , with the corresponding theoretical errors [2]. Results of the analysis with two free parameters:  $m^2$  and  $\tan^2 \theta$  are shown in Fig. 3. In the best  $\chi^2$  point:

$$m^2 = 7.36 \cdot 10^5 \text{ eV}^2; \quad \tan^2 \theta = 0.41 \quad (12)$$

we have  $\chi^2 = 74.0 = 82$ . The allowed region is shifted to larger  $\tan^2 \theta$  in comparison with the free  $f_B$  fit. Indeed, in the latter case we had  $f_B > 1$ , so to compensate the decrease of  $f_B$  the survival probability, which is proportional to  $\sin^2 \theta$ , should increase. Also the contours of constant confidence level shift to larger mixings. The 3  $\sigma$  upper bound becomes weaker:  $\tan^2 \theta < 0.628$ .

Notice that the h-LMA region is rejected now at the 3 level.

## 4 Effect of 1-3 mixing

As it was found in the pre-salt phase analysis, the 1-3 mixing improves the relative goodness of the fit in the h-LMA region (see, e.g., [19]). Can non-zero 1-3 mixing substantially change the results of sect. 3?

Both for the KamLAND and for solar neutrinos the oscillations driven by  $m_{13}^2$  are averaged out and signals are determined by the survival probabilities

$$P_{ee} = (1 - \sin^2 \theta_{13})^2 P_2 + \sin^4 \theta_{13} + (1 - 2 \sin^2 \theta_{13}) P_2; \quad (13)$$

where  $P_2 = P_2(m_{12}^2; \theta_{12})$  is the two neutrino vacuum oscillation probability in the case of KamLAND and it is the matter conversion probability in the case of solar neutrinos.

The effect of non-zero 1-3 mixing is reduced to the overall suppression of the survival probability. According to recent analysis of the atmospheric neutrino data [23] the allowed region of oscillation parameters has shifted to smaller  $m_{13}^2$ , and consequently, the upper bound on 1-3 mixing from the CHOOZ experiment [24] becomes weaker:  $\sin^2 \theta_{13} = 0.067$  (3%) [25]. For this value of  $\sin^2 \theta_{13}$ , the suppression can reach 13% in (13). The influence of  $\sin^2 \theta_{13}$  on the global fit can be traced in the following way.

There are three sets of observables for which effects of  $\sin^2 \theta_{13}$  are different.

1) Total rates (fluxes) at high energies measured by SNO and SK. These rates depend essentially on the combination  $\cos^4 \theta_{13} P_2$ . In particular,

$$\frac{CC}{NC} = \cos^4 \theta_{13} P_2; \quad \frac{ES}{NC} = \cos^4 \theta_{13} P_2 (1 - r) + r; \quad (14)$$

The ratios of fluxes are unchanged if

$$\cos^4 \theta_{13} h P_2(m_{12}^2; \tan^2 \theta_{12}) = \text{const}; \quad (15)$$

where  $h$  is the averaging over the relevant energy range. The product (15) is invariant with increase of  $\sin^2 \theta_{13}$  (decrease of  $\cos^4 \theta_{13}$ ) if the probability increases. In the region near the b.f. point (8) the latter requires increase of  $m_{12}^2$  or/and  $\tan^2 \theta_{12}$ . Then the absolute values of fluxes can be reproduced by tuning  $f_B$  (in the free  $f_B$  fit).

With increase of  $\sin^2 \theta_{13}$  the predicted spectrum becomes flatter which does not change the quality of fit significantly.

The day-night asymmetry decreases with increase of  $m_{12}^2$  which is slightly disfavored by the data. Future more precise measurements of asymmetry will have stronger impact.

2) Low energy observables, sensitive to pp- and Be- neutrino fluxes. They depend on the averaged vacuum oscillation probability. In particular, the Ge-production rate is proportional to

$$Q_{Ge} / \cos^4 \theta_{13} (1 - 0.5 \sin^2 \theta_{12}); \quad (16)$$

Notice that practically there is no dependence of these observables on  $m_{12}^2$ . Since in the best fit point for zero 1-3 mixing  $Q_{\text{theor}} = Q_{\text{exp}}$ , a significant increase of  $\sin^2_{13}$  will lead to worsening of the fit (though small non-zero 1-3 mixing,  $\sin^2_{13} < 0.04$ , could be welcomed).

3) KamLAND. The present best fit point is near the maximum of oscillation survival probability averaged over the atomic reactors. So, the increase of 1-3 mixing could be compensated by the decrease of 1-2 mixing.

These features allow one to understand results of the data fit.

We have performed analysis of the solar neutrino data for fixed value  $\sin^2_{13} = 0.067$  (Fig. 4). The number of degrees of freedom is the same as in the 2 fit and we follow the procedure described in Sect. 3 with survival probabilities given in (13). The best fit point

$$m^2 = 11.0 \cdot 10^5 \text{eV}^2; \quad \tan^2 \theta = 0.38; \quad f_B = 1.03 \quad (17)$$

corresponds to  $\chi^2_{\text{dof}} = 66.8/81$ . It is shifted to larger  $m^2$  to satisfy condition (15). The shift to larger 1-2 mixing is disfavored by the Gallium experimental results (16). The allowed region is also shifted to larger  $m^2$  and its size increases (also in the mixing direction). These results agree with the analysis in [15].

We also performed the combined analysis of the solar neutrino data and the KamLAND spectrum for  $\sin^2_{13} = 0.067$ . In the best fit point we find  $\chi^2_{\text{min}}/\text{dof} = 74.3/94$  and

$$m^2 = 7.1 \cdot 10^5 \text{eV}^2; \quad \tan^2 \theta = 0.42; \quad f_B = 1.03 \quad (18)$$

So, introduction of the 1-3 mixing slightly worsen the fit:  $\chi^2_{\text{min}} = 1.9$ . The best fit point shifts to larger  $\tan^2 \theta$  to satisfy the condition (15). Significant shift to larger  $m^2$  is not allowed by the KamLAND spectral data. At the same time, the 1-3 mixing improves a fit in the h-region. This region is accepted now at 90 % C.L. with respect to the best fit point (18).

Notice however, that such an improvement is realized for values of  $\sin^2_{13}$  which are accepted by the CHOOZ and atmospheric data at the 3 level. So, inclusion of the CHOOZ result in the global fit changes a situation and no significant improvement of the fit in the h-LMA region occurs [18]. In fact, at  $\sin^2_{13} = 0.067$  this region disappears even at the 3 level.

## 5 Physics of the solar neutrino conversion.

### 5.1 Dynamics of conversion

With new SNO results the h-LMA region is excluded or strongly disfavored and also significant deviation of 1-2 mixing from maximum is established. This essentially determines

both qualitatively and now quantitatively the physical picture of solar neutrino conversion (see also [26]). Different analyzes of data converge to

$$m^2 = (6 - 8) \cdot 10^5 \text{eV}^2; \quad \sin^2 \theta = 0.28 - 0.30; \quad (19)$$

The non-zero  $1-3 \text{ m}$  mixing may produce some small shift of the parameters. Since the physical picture is nearly the same for all points in these intervals, for further estimations we will take the values (8) as the reference point.

We take the difference of the matter potentials for  $\nu_e$  and  $\nu_a$  (active) according to the Standard Model:

$$V = \frac{\rho}{2G_F} Y_e m_N; \quad (20)$$

Here  $\rho$  is the matter density,  $Y_e$  is the number of electrons per nucleon, and  $m_N$  is the nucleon mass. In fact, the latest experimental data allow to check the presence of such a potential in the model independent way. The extracted value of the potential is in agreement with (20) (within 1%) and  $V = 0$  is rejected at 5.6% level [14].

For parameters (19) the neutrino evolution inside the Sun occurs in the highly adiabatic regime. It is convenient to write the averaged adiabatic survival probability as [3, 4]

$$P = \sin^2 \theta + \cos 2\theta \cos^2 \theta_m^0; \quad (21)$$

where  $\theta_m^0$  is the mixing angle in the production point. Provided that there is no coherence lost (see discussion at the end of the section), the depth of oscillations at the surface of the Sun equals [4]

$$A_P = \sin 2\theta \sin 2\theta_m^0; \quad (22)$$

So that the probability (being the oscillatory function of distance) is inscribed in the following oscillation strip

$$P = \frac{1}{2} \sin 2\theta \sin 2\theta_m^0; \quad (23)$$

The oscillation length in matter,  $l_m$ , is smaller than the resonance oscillation length,  $l_R = l / \sin 2\theta$ , where  $l$  is the vacuum oscillation length. So, for typical energy 10 MeV we find  $l_m = 3.5 - 10 \text{ m}$ . Along the solar radius,  $R$ , about  $R / l_m = 2 - 10$  oscillation length are obtained, and consequently, the oscillations are strongly averaged out.

Dynamics of the effect depends on  $\sin^2 \theta$  and

$$(E) \quad \frac{E_{\text{kin}}}{V_0} = \frac{m^2}{2E V_0} = \frac{m^2 m_N}{2 \rho G_F (Y_e)_0}; \quad (24)$$

which is the ratio of the "kinetic" energy,  $m^2 = 2E$ , and the potential energy in the neutrino production point,  $V_0$ . For a given energy,  $(E)$  determines the relative contributions of the vacuum oscillation and the matter effect.



## 5.2 Two limits

Depending on  $\theta_m$  there are two limits:

1. Matter dominance:  $\theta_m \rightarrow 1$  which corresponds to  $E \rightarrow 1$ . In this limit the neutrino flavor evolution has a character of the non-oscillatory ( $A_P = 0$ ) conversion with the survival probability [4]:

$$P_{\text{non-osc}} = \sin^2 \theta : \quad (25)$$

In this case neutrinos produced far above the resonance density propagate to zero (small) density adiabatically. The initial mixing is strongly suppressed ( $\theta_m \rightarrow 0$ ) and the propagating neutrino state practically coincides with the heaviest eigenstate:  $\nu(t) = \nu_{2m}$ . At the exit from the Sun:  $\nu(t) = \nu_2$  [4].

2. Vacuum dominance:  $\theta_m \rightarrow 0$  which corresponds to  $E \rightarrow 0$ . Matter effects are small. The flavor evolution has a character of vacuum oscillations, so  $P$  converges to the averaged oscillation probability

$$P \rightarrow P_{\text{vac}} = 1 - 0.5 \sin^2 2\theta ; \quad (26)$$

and  $A_P \rightarrow \sin^2 2\theta$ .

For the reference value of mixing (8) we find

$$P_{\text{non-osc}} = 0.281; \quad P_{\text{vac}} = 0.596: \quad (27)$$

The resonance value of  $\theta$ , for which  $P = 1/2$ , equals

$$\theta_R = \frac{1}{\cos 2\theta} = 2.28: \quad (28)$$

It marks the transition region between the two extreme cases.

The boron neutrinos are produced in the region where the density  $Y_e$  decreases from 100 to 70 g/cc. The layer with maximum of emissivity ( $r = 0.043R_\odot$ ) has the effective density  $Y_e = 93.4$  g/cc [2]. For this density the value (28) corresponds to the resonance energy  $E_R = 2.2$  MeV. Neutrinos with  $E < E_R$  ( $E > 2.2$  MeV) are produced above the resonance (density) and then propagating to the surface of the Sun cross the resonance layer. Neutrinos with  $E > E_R$  ( $E < 2.2$  MeV) are produced below the resonance (density) and never cross the resonance (or cross the resonance layer twice depending on direction of propagation).

We can also define the "median" energy at which the probability equals the average of the two asymptotics (25) and (26):  $P_{\text{med}} = 0.5(P_{\text{vac}} + P_{\text{non-osc}})$ . According to (21), this corresponds to  $\cos^2 \theta_m = 0.5 \cos^2 \theta$  and is realized for

$$\theta_{\text{med}} = \cos 2\theta + \frac{2 \sin^3 \theta}{1 + \sin^2 \theta} : \quad (29)$$

We find that  $m_{\text{ed}} = 1.43$  and  $E_{\text{med}} = 3.54 \text{ MeV}$ .

The ratio  $CC/NC$  measured by SNO determines the survival probability averaged over the energy range above the SNO threshold for the CC events ( $E > 5 \text{ MeV}$ ):

$$\frac{CC}{NC} = \langle P \rangle \quad (30)$$

For the reference value (8) we get  $\langle P \rangle = 0.322$ . This value is slightly larger than the experimental result (1).

So, both the experimental and theoretical values of  $CC/NC$  are rather close to  $P_{\text{non-osc}}$  which means that at high energies ( $E > 5 \text{ MeV}$ ) the evolution of neutrino state is nearly non-oscillatory conversion. The difference

$$\frac{CC=NC}{P_{\text{non-osc}}} - 1 = \frac{CC=NC}{\sin^2} - 1 = 0.13 \quad (31)$$

is due to

the averaged oscillation effect inside the Sun. In fact, for  $(Y)_0 = 93.4 \text{ g/cc}$  and energies relevant for the SNO CC signal,  $E = 14; 10; 6 \text{ MeV}$ , we obtain  $\langle P \rangle = 0.36; 0.50; 0.84$  correspondingly. These values of  $\langle P \rangle$  are not small, though being smaller than the resonance value. Therefore one may expect a significant deviation of  $P$  from the asymptotic value.

the earth regeneration effect.

### 5.3 Survived probability: adiabatic conversion versus oscillations

The survival probability can be written as

$$P = \sin^2 + P_{\text{reg}} + P_{\text{osc}}; \quad (32)$$

where  $P_{\text{reg}}$  is the regeneration correction and  $P_{\text{osc}}$  is the oscillation correction. Both these corrections are positive.

The regeneration effect,  $P_{\text{reg}}$ , can be expressed in terms of the Day-Night asymmetry,  $A_{\text{DN}}$ , as:

$$P_{\text{reg}} = A_{\text{DN}} \frac{P_{\text{non-osc}} \sin^2}{M_D} \quad (33)$$

For the best fit point the asymmetry equals  $A_{\text{DN}} = 3.0\%$ , and consequently,  $P_{\text{reg}} = 0.008$ .

Using formula for the adiabatic conversion (21) we find:

$$P_{\text{osc}} = \cos^2 \cos^2 \frac{\theta}{m} : \quad (34)$$

Notice that  $\cos^2 \theta_m^0$  gives the probability to find the eigenstate  $\nu_{1m}$  in the adiabatically propagating neutrino state:  $\langle \nu_{1m} | \psi(t) \rangle^2 = \cos^2 \theta_m^0 = \text{const.}$  In the non-oscillatory limit we would have  $\cos^2 \theta_m^0 = 0$  and  $\psi(t) = \nu_{2m}$ . The presence of second eigenstate,  $\nu_{1m}$ , in  $\psi(t)$ , leads to the interference effect, and consequently, to oscillations.

In the limit of small  $\epsilon$  we find

$$\cos^2 \theta_m^0 = \frac{1}{4} \sin^2 2\theta + \epsilon^2; \quad (35)$$

and therefore the correction to probability can be written as

$$P_{\text{osc}} = \frac{1}{4} \cos 2\theta \sin^2 2\theta (\epsilon^2 + O(\epsilon^3)); \quad (36)$$

Notice that the correction is quadratic in  $\epsilon$ , and furthermore, it contains small pre-factor  $\cos 2\theta = 0.1$ . It is for this reason the correction is rather small in spite of large values of  $\epsilon$ . However, convergence of the series is determined by  $\epsilon$  itself, and so, the corrections to the first order  $P_{\text{osc}}$  are not small. Although (36) allows to understand the size of the correction, in our estimations we use exact expression for  $\cos^2 \theta_m^0$ . In the limit of small the depth of oscillations

$$A_P \propto \sin^2 2\theta \quad (37)$$

decreases linearly, that is, slower than correction to the average value.

In fig. 5 the averaged survival probability is shown as a function of the neutrino energy for different production points (different initial densities). The shadowed strips show the depth which oscillations would have at the surface of the Sun, provided that there is no loss of coherence. The average  $P$  converges to  $P_{\text{non-osc}}$  (dashed line) with increase of energy and  $Y_e$ . The decrease of oscillation depth with  $Y_e$  is much slower than convergence of  $P$  to  $\sin^2 \theta$ :  $P \propto \epsilon^2$ ,  $A_P \propto \epsilon$ . The depth of oscillations increases with decrease of  $E$  approaching the vacuum value. Notice that even for the highest energies of the spectrum the conversion is not completely non-oscillatory, though  $P \propto \sin^2 \theta$ .

Using  $\epsilon = 0.50$  which corresponds to a typical energy of the spectrum measured by SNO,  $E = 10 \text{ MeV}$ , we get  $P_{\text{osc}} = 0.030$  (approximate formula (36) leads to  $P_{\text{osc}} = 0.022$ ). This together with the regeneration effect reproduces well the observed difference of  $P$  and  $P_{\text{non-osc}}$ . The depth of oscillations for this set of parameters is rather large:  $A_P = 0.45$ .

Thus, at energies relevant for the SNO CC events, the survival probability is about 12% larger than the non-oscillatory probability. Oscillations give dominating effect in this difference. The regeneration contributes about 4%.

At low energies ( $E < 2 \text{ MeV}$ ) the Earth regeneration ( $\propto (\sin^2 \theta = E)^2$ ) can be neglected and the probability is given by the vacuum oscillation formula with small matter corrections. For  $\epsilon \ll 1$  we can write:

$$P = P_{\text{vac}} + \frac{1}{2} \cos 2\theta \sin^2 2\theta \epsilon^2; \quad (38)$$

For the beryllium neutrinos the effective density in the production region  $(Y_e)_0 = 87 \text{ g/cc}$ , and correspondingly,  $\rho = 6.28$ . Inserting this value of  $\rho$  in (38) we find  $P = 0.028$  which is smaller than 5% of  $P_{\text{vac}}$ .

For the pp-neutrinos the effective density in the region of the highest production rate is  $(Y_e)_0 = 68 \text{ g/cc}$ . At  $E = 0.4 \text{ MeV}$  this gives  $\rho = 17.3$  and correction  $P = 0.01$ .

The results for different values of  $m^2$  can be immediately obtained from Fig. 5 by rescaling of the energy: for  $m^2$  the probability at the energy  $E^0$  equals  $P(E^0) = P(E)$  where  $E = E^0 (\rho^2 = \rho_0^2)$ . If, e.g.,  $m^2 = 14 \cdot 10^5 \text{ eV}^2$ , we find from Fig. 5, that  $P = 0.46; 0.40; 0.35$  for  $E = 6; 10; 14 \text{ MeV}$ . Notice that even for so large  $m^2$ , the probability is substantially lower than the vacuum value and for high energies the matter effect still dominates.

## 5.4 Coherence loss

Let us consider effect of the coherence loss of a neutrino state on the conversion picture. The loss of coherence suppresses depth of oscillations, so that the probability converges to the average value.

The coherence length,  $L_{\text{coh}}$ , can be estimated from the condition:

$$\int_0^{L_{\text{coh}}} dx \, v_m = \pi; \quad (39)$$

where  $v_m = v_{2m} - v_{1m}$  is the difference of the group velocities of the eigenstates,  $L$  is the length of the wave packet and  $x$  is the distance. The group velocities equal:

$$v_{im} = \frac{dH_{im}}{dp}; \quad i = 1, 2; \quad (40)$$

where  $H_i$  are the eigenvalues of the effective Hamiltonian of the neutrinos in matter. For the difference of the velocities we find [27]:

$$v_m = \frac{m^2}{2p^2} \frac{x \cos 2\theta}{\frac{x^2}{4} \cos^2 2\theta + 1}; \quad (41)$$

where  $x = m^2 = 2pV(x)$ .

Let us analyze the expression in (41). In vacuum,  $x \rightarrow 0$  and

$$v_m = v = \frac{m^2}{2p^2}; \quad (42)$$

With increase of density the difference  $v_m$  decreases. In the resonance we find

$$v_m = \frac{m^2}{2p^2} \sin^2 \theta; \quad (43)$$

$v_m$  changes the sign at  $x = \cos 2$  which corresponds to density  $\rho_0 = \rho_R = \cos^2 2$  larger than the resonance density. For  $\rho > \rho_0$  the difference of velocities changes sign. At very high densities,  $x \rightarrow 0$ , we have

$$v_m = \frac{m^2}{2p^2} \cos 2 : \quad (44)$$

Notice that in the resonance channel always  $|v_m| < |v|$ . So, the matter suppresses the divergence of packets. Furthermore, due to change of sign of  $v_m$  the overlap of packets can be recovered. If neutrino propagates from high densities (above the resonance) the packets first diverge, but then below  $\rho_0$  the overlap and therefore the coherence can be restored again.

For the smallest value of  $v = 0.36$  in our case ( $E = 14 \text{ MeV}$ ,  $\rho = 94 \text{ g/cc}$ ) we get  $v_m = 0.08 v$ . So, the divergence effect can be estimated using the vacuum value

$$L_{\text{coh}} = \frac{2E^2}{m^2} : \quad (45)$$

The sizes of wave packets are different for different components of the solar neutrino spectrum. Let us consider them in order.

The lifetime of isolated  $^8\text{B}$  nuclei,  $\tau_B = 10^8 \text{ s}$ , is very long and the size of the wave packet is determined by the average time between two consequent collisions,  $t_{\text{coll}}$ :

$$L_{\text{coh}} = \tau_{\text{coll}} : \quad (46)$$

Furthermore, the collisions with large enough momentum transfer  $p$ :

$$p > \frac{2}{\lambda} \quad (47)$$

should be considered. For smaller  $p$  the collision does not break coherence (shorten the packet). Using Eq. (46) and (47) we find the condition for  $\lambda$ :

$$\tau_{\text{coll}} > \frac{2}{\lambda} : \quad (48)$$

The collision time can be estimated as

$$t_{\text{coll}} = \frac{1}{(p)v n} ; \quad (49)$$

where  $v$  is the velocity of colliding particles (protons, electrons, the helium atoms),  $n = n_N$  is the number density of these particles and  $\sigma(p)$  is the cross-section. The dominating effect is the Coulomb scattering, so that the cross-section can be written as

$$\sigma(p > \frac{2}{\lambda}) = \frac{A}{(p)^2} = \frac{A^2}{(2)^2} ; \quad (50)$$

where in the lower approximation  $A \propto (Z/v)^2$  corresponds to the Rutherford formula, where  $Z = 5$  is the charge of Boron nuclei,  $v^2=4$  and  $v$  is the velocity of a colliding particle. In our case  $Z/v > 1$  and the perturbation theory is violated. For estimations we take  $A \approx 0.1$ . Inserting (50) into (49) and then (48) we get

$$= \frac{4 \sum_{l=3}^{\infty} l^2}{nvA} \quad (51)$$

which leads to

$$= (1.2) \cdot 10^7 \text{ cm} : \quad (52)$$

This result is in agreement with results obtained by other methods [28, 29, 30]. The coherence length equals:

$$L_{\text{coh}} \approx (4-8)R \frac{E}{10 \text{ MeV}}^2 : \quad (53)$$

Here  $R = 7 \cdot 10^8 \text{ cm}$  is the solar radius. The matter effect leads to suppression of the divergence, and consequently, to larger coherence length. According to (51) for the observable part of the boron neutrino spectrum the effect of the coherence loss is small. Strong divergence of packets in the conversion region ( $x \approx 0.1R$ ) occurs for  $E < 1.5 \text{ MeV}$ .

For the  ${}^7\text{Be}$  neutrinos the length of wave packet is determined by the production time [30], that is by the capture of the electron. The latter is given by the time an electron wave packet of the size  $\lambda_e$  crosses nucleus [30]:

$$t = \frac{\lambda_e}{v_e} : \quad (54)$$

Using the thermal velocity:  $v_e = \sqrt{\frac{3kT}{m_e}}$  and the thermal wave length for the electron packet:  $\lambda_e = \frac{h}{m_e v_e}$ , we get from (54) for the neutrino wave packet length:

$$\frac{2}{m_e v_e^2} = \frac{2}{3kT} : \quad (55)$$

Numerically this gives  $6 \cdot 10^8 \text{ cm}$  [30].

The  $\text{Be}$  neutrinos undergo nearly vacuum oscillations with small matter effect, so to calculate the coherence length we can use the formula (45):

$$L_{\text{coh}}(\text{Be}) \approx 0.01R : \quad (56)$$

That is, the coherence is lost already in the production region. Notice that the oscillation length is even smaller ( $3 \cdot 10^8 \text{ cm}$ ) and  $L_{\text{coh}} \approx 1/200$ .

For the  $pp$ -neutrinos the coherence length is given by (45). The size of the packets is determined by the time of interaction which, in turn, is given by the wave packet of the colliding proton, similarly to the case of  ${}^7\text{Be}$  neutrinos. Notice that expression (55) does

not depend on a mass of colliding particle, and therefore it can be immediately applied for the pp-neutrinos. As a result, the neutrino wave packet has the same size  $\sim 6 \cdot 10^6$  cm. The coherence length is shorter due to smaller energies:

$$L_{\text{coh}}(\text{pp}) \approx 0.002R \frac{E}{0.4 \text{ MeV}}^2 ; \quad (57)$$

Again the loss of coherence occurs already in the production region. The number of oscillation periods before complete averaging:  $L_{\text{coh}} = l < 100$ .

## 6 Spectrum distortion at SNO

Distortion of the energy spectrum is the generic consequence of the LMA-MSW solution. As we discussed in the previous section, with decrease of energy the survival probability increases due to increase of the oscillation contribution.

The energy spectrum of electrons has been calculated according to

$$S(T_{\text{eff}}) = \int_{T_r}^Z \int_E^Z \frac{d(T_r; E)}{dT_r} R(T_r; T_{\text{eff}}) P^B f_B(E) + P^{\text{hep}} f_{\text{hep}}(E) dE dT_r ; \quad (58)$$

where  $T_{\text{eff}}$  is the measured electron kinetic energy,  $T_r$  is the real electron kinetic energy,  $E$  is the neutrino energy,  $f_B$  ( $f_{\text{hep}}$ ) is the Boron (hep) neutrino flux,  $d(T_r; E) = dT_r$  is the differential cross section taken from [31], and  $R(T_r; T_{\text{eff}})$  is the SNO resolution function,  $P^B$  and  $P^{\text{hep}}$  are the survival probabilities averaged over the corresponding production regions.

In Fig. 6 we show the results of calculations of spectra for different values of  $m^2$ . The distortion due to oscillations which dominates at low energies is partly compensated by the regeneration effect at high energies. Thus, for the day signal one expects stronger upturn.

According to Fig. 6, the upturn is about 8–15%. We show also the SNO experimental points from the salt phase. A dependence of the distortion on  $m^2$  is rather weak in the allowed region. Notice that in the low energy part the spectrum has a tendency to turn down in contrast to the expected effect. At  $E < 7.5$  MeV the points are systematically below the predicted rate. One should notice, however, that the experimental points include the statistical error only and it is not excluded that some systematics explains the observed result.

The same effect – an absence of the upturn of the spectrum – is observed in the phase –I of the SNO experiment [5]. The spectral data agree well with the undistorted spectrum. It would be interesting to combine the results of both phases to improve statistics (and probably reduce the number of bins). Being confirmed, the fact of absence of the upturn or even a turn down at low energies can be explained by the effect of additional sterile neutrino [32].

## 7 Next step

Let us present predictions for the forthcoming experiments.

1). KamLAND. More precise measurements of the rate and spectrum distortion are expected. That can further diminish uncertainty in the determination of  $m^2$ . In g. 7 we show the contours of constant suppression of the KamLAND rate  $R_{KL}$  above 2.6 MeV:

$$R_{KL} = \frac{N(m^2; \tan^2)}{N_0}; \quad (59)$$

where  $N$  and  $N_0$  are the numbers of events with and without oscillations. As follows from the figure strengthening of the lower bound on  $R_{KL}$  will cut the allowed region from the side of small  $m^2$  ( $5 - 10 \text{ eV}^2$ ) as well as large  $m^2$  ( $9 - 10 \text{ eV}^2$ ) and large mixings:  $\tan^2 \approx 0.45$ . In contrast, strengthening of the upper bound on  $R_{KL}$  will disfavor the region of small mixings:  $\tan^2 \approx 0.3$ .

The spectrum distortion can be characterized by a relative suppression of rates at the high and low energies. We choose  $E = 4.3 \text{ MeV}$  as the border line [19], so that the interval (2.6–4.3) MeV contains 4 energy bins. Introducing the rates  $R_{KL}(< 4.3 \text{ MeV})$  and  $R_{KL}(> 4.3 \text{ MeV})$  we define the shape parameter as

$$k = \frac{1 - R_{KL}(> 4.3 \text{ MeV})}{1 - R_{KL}(< 4.3 \text{ MeV})}; \quad (60)$$

$k$  does not depend on the normalization of spectrum and on the mixing angle in the 2 context. It increases with the oscillation suppression of signal at high energies.  $k > 1$  ( $k < 1$ ) means stronger suppression at high (low) energies. The present KamLAND data give [19]

$$k^{\text{exp}} = 0.84^{+0.42}_{-0.35}; \quad 1 : \quad (61)$$

In g. 7 we show the contours of constant shape parameter. According to this figure at the 1 level

$$k^{\text{th}} = 1.05^{+0.75}_{-0.50} \quad (62)$$

in a very good agreement with (61). In the h-LMA (1) region we find  $k = 0.5 - 2.3$ . So that even mild increase of statistics will influence the allowed range of  $m^2$ .

In the h-LMA region the allowed interval,  $k = 0.9 - 1.4$ , is narrower. So, if forthcoming measurements favor  $k < 0.9$  or  $k > 1.4$ , the h-LMA region will be further discriminated.

2). Precise measurements of the CC/NC ratio at SNO. In g. 8 we show the contours of constant CC/NC ratio with finer grid than before. We find predictions for the best fit point and the 3 interval:

$$\frac{CC}{NC} = 0.32^{+0.08}_{-0.07}; \quad (3) : \quad (63)$$



3). The day-night asymmetry at SNO. In fig. 8 we show also the contours of constant  $A_{DN}^{SNO}$  for the energy threshold 5.5 MeV. The best fit point prediction and the 3 bound equal

$$A_{ND}^{SNO} = 3.0 \pm 0.8\% ; (1\sigma); A_{ND}^{SNO} < 6\% (3\sigma); \quad (64)$$

4). Germanium production rate. In the best fit point we predict  $Q_{Ge} = 71$  SNU. We show in fig. 9 the lines of constant Ge production rate with finer (than before) grid.

For the Argon production we have  $Q_{Ar} = 2.96$  SNU in the global b.f. point. We show in fig. 9 also the lines of constant Argon production rate.

## 8 Conclusions

1. The SNO-II fluxes have only slightly shifted the best fit point toward smaller  $m^2$  and  $\tan^2$ . The most important improvements consist however of the stronger upper bounds on  $m^2$  and  $\tan^2$ . Those imply that the h-LMA region is strongly disfavored and 1-2 mixing deviates substantially from the maximal one:

$$(\sin^2 2\theta < 0.5) \quad \sin^2 \theta : \quad (65)$$

The 1-3 mixing does not change these results once the CHOOZ data are included in the analysis.

2. These improvements in measurements of the oscillation parameters lead to a situation when physics of the solar neutrino conversion is essentially (and quantitatively) determined. In the high energy part of spectrum the averaged survival probability is close to the non-oscillatory one. For  $E > 5$  MeV the effective  $P$  is about 12% higher than  $\sin^2 \theta$ . Oscillations give the dominant contribution to this difference:  $\approx 8-14\%$ , the rest is due to the Earth regeneration effect. In spite of smallness of difference ( $P - \sin^2 \theta$ ) which is proportional to  $\theta^2$ , the depth of oscillations is relatively large:  $A_p \approx 0.45$  being proportional to  $\theta$ . At low energies ( $E < 1$  MeV), vacuum oscillations are the dominant process with the matter corrections to  $P$  below 5%.

3. After the SNO salt results the errors of determination of the oscillation parameters become smaller than the values of parameters:

$$(m^2) < m^2; \quad (\tan^2 \theta) < \tan^2 \theta : \quad (66)$$

This means that the solar neutrino studies enter a stage of precision measurements.

For the forthcoming measurements we predict about 8 - 15% upturn of the energy spectrum at SNO. If further measurements confirm the absence of the upturn hinted by the present data, some physics "beyond LMA" should be invoked.

The CC/NC ratio is expected to be  $0.32$ , the Day-Night asymmetry:  $A_{ND}^{SNO} \approx 3\%$  ( $T_{eff} > 5.5$  MeV), the spectrum shape parameter:  $k = 1.0 \pm 0.8 = 0.5$ .

## 9 Acknowledgments

One of the authors (P.C.H.) would like to thank FAPESP for financial support. The work of A.S. was supported by the TM R, EC-contract No. HPRN-CT-2000-00148 and No. HPRN-CT-2000-00152.

## References

- [1] SNO collaboration (Q.R.Ahmad et al.), nucl-ex/0309004.
- [2] J.N.Bahcall, M.H.Pinsonneault and S.Basu, *Astrophys. J.* 555, 990 (2001).
- [3] L.Wolfenstein, *Phys.Rev.D* 17, 2369 (1978); L.Wolfenstein, in "Neutrino-78", Purdue Univ. C3-C6, (1978).
- [4] S.P.Mikheyev and A.Yu.Smirnov, *Yad.Fiz.* 42, 1441 (1985) [*Sov.J.Nucl.Phys.* 42, 913 (1985)]; *Nuovo Cim.* C 9, 17 (1986); S.P.Mikheyev and A.Yu.Smirnov, *ZHETF*, 91, (1986), [*Sov.Phys. JETP*, 64, 4 (1986)] (reprinted in "Solar neutrinos: the first thirty years", Eds. J.N.Bahcall et. al.).
- [5] SNO collaboration, Q.R.Ahmad et al.; *ibidem* 87, 071301 (2001); *ibidem* 89, 011301 (2002); *ibidem* 89, 011302 (2002).
- [6] B.T.Cleveland et al., *Astroph. J.* 496, 505 (1998).
- [7] SAGE collaboration, J.N.Abdurashitov et al. *Zh.Eksp. Teor. Fiz.* 122, 211 (2002) [*J. Exp. Theor. Phys.* 95, 181 (2002)], astro-ph/0204245; V.N.Gavrin, Talk given at the V IIIth International conference on Topics in Astroparticle and Underground Physics (TAUP 03), Seattle, Sept. 5-9, 2003.
- [8] GALLEX collaboration, W.Hampel et al., *Phys.Lett.B* 447, 127 (1999).
- [9] GNO Collaboration, E.Belotti, Talk given at the V IIIth International conference on Topics in Astroparticle and Underground Physics (TAUP 03), Seattle, Sept. 5-9, 2003.
- [10] Super-Kamiokande collaboration, S.Fukuda et al., *Phys. Rev. Lett.* 86, 5651 (2001); *Phys. Rev. Lett.* 86, 5656 (2001), *Phys. Lett.B* 539, 179 (2002).
- [11] Super-Kamiokande collaboration, M.B.Smy et al., hep-ex/0309011.
- [12] KamLAND collaboration, K.Eguchi et al., *Phys. Rev. Lett.* 90, 021802 (2003).
- [13] A.B.Balantekin and H.Yuksel, hep-ph/0309079.
- [14] G.L.Fogli, E.Lisi, A.Marrone, A.Palazzo, hep-ph/0309100.

- [15] M. Maltoni, T. Schwetz, M. A. Tortola, J. W. F. Valle, hep-ph/0309130 (v2).
- [16] P. Aliani, V. Antonelli, M. Picariello, E. Torrente-Lujan, hep-ph/0309156.
- [17] P. Cremine, G. Signorelli, A. Strumia, hep-ph/0102234, v5, Sept. 15 (2003).
- [18] A. Bandyopadhyay, S. Choubey, S. Goswami, S. T. Petcov, D. P. Roy, hep-ph/0309174.
- [19] P. C. de Holanda, A. Yu. Smirnov, JCAP 0302, 001 (2003).
- [20] "HOW TO use the SNO salt ux results", website: [www.sno.phy.queensu.ca](http://www.sno.phy.queensu.ca).
- [21] L. E. Marcucci et al., Phys. Rev. C 63 (2001) 015801; T.-S. Park, et al., nucl-th/0107012, nucl-th/0208055 and references therein.
- [22] P. C. de Holanda, A. Yu. Smirnov, Phys. Rev. D 66, 113005 (2002).
- [23] Super-Kamiokande Collaboration, Y. Hayato, talk given at the HEP 2003 International Europhysics Conference (Aachen, Germany, 2003), website: [eps2003.physik.rwth-aachen.de](http://eps2003.physik.rwth-aachen.de).
- [24] CHOOZ Collaboration, M. Apollonio et al., Phys.Lett. B 466, 415 (1999); Eur. Phys. J., C 27, 331 (2003).
- [25] G. L. Fogli, E. Lisi, A. Marrone, D. Montanino, A. Palazzo, A. M. Rotunno, hep-ph/0308055.
- [26] A. Yu. Smirnov, Invited talk at 10th International Workshop on Neutrino Telescopes, Venice, Italy, 11-14 Mar 2003, hep-ph/0305106.
- [27] S. P. Mikheyev and A. Yu. Smirnov, Prog. in Part. and Nucl. Phys. 23 (1989) 41.
- [28] S. Nussinov, Phys. Lett. B 63 (1976) 201.
- [29] A. Loeb, Phys. Rev. D 39 (1989) 1009.
- [30] K. Kiers, S. Nussinov and N. Weiss, Phys. Rev. D 53 (1996) 537-547.
- [31] S. Nakamura et. al, Nucl. Phys. A 707, 561 (2002).
- [32] P. C. de Holanda, A. Yu. Smirnov, hep-ph/0307266.

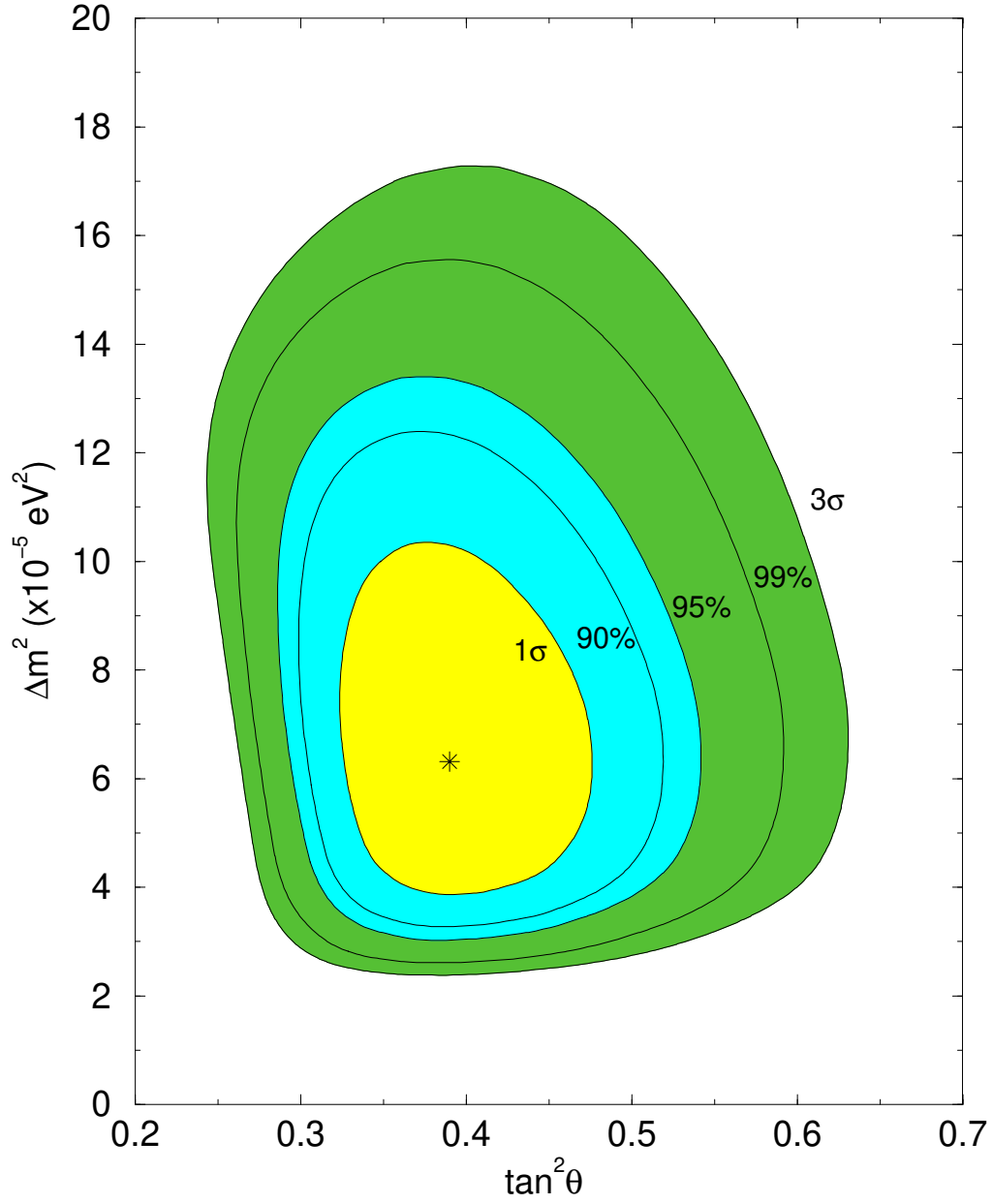


Figure 1: The allowed regions in  $\tan^2\theta$  -  $m^2$  plane, from a combined analysis of the solar neutrino data at 1 , 90% , 95% , 99% and 3 C.L.. The boron neutrino flux is treated as free parameter. The best fit point is marked by star.

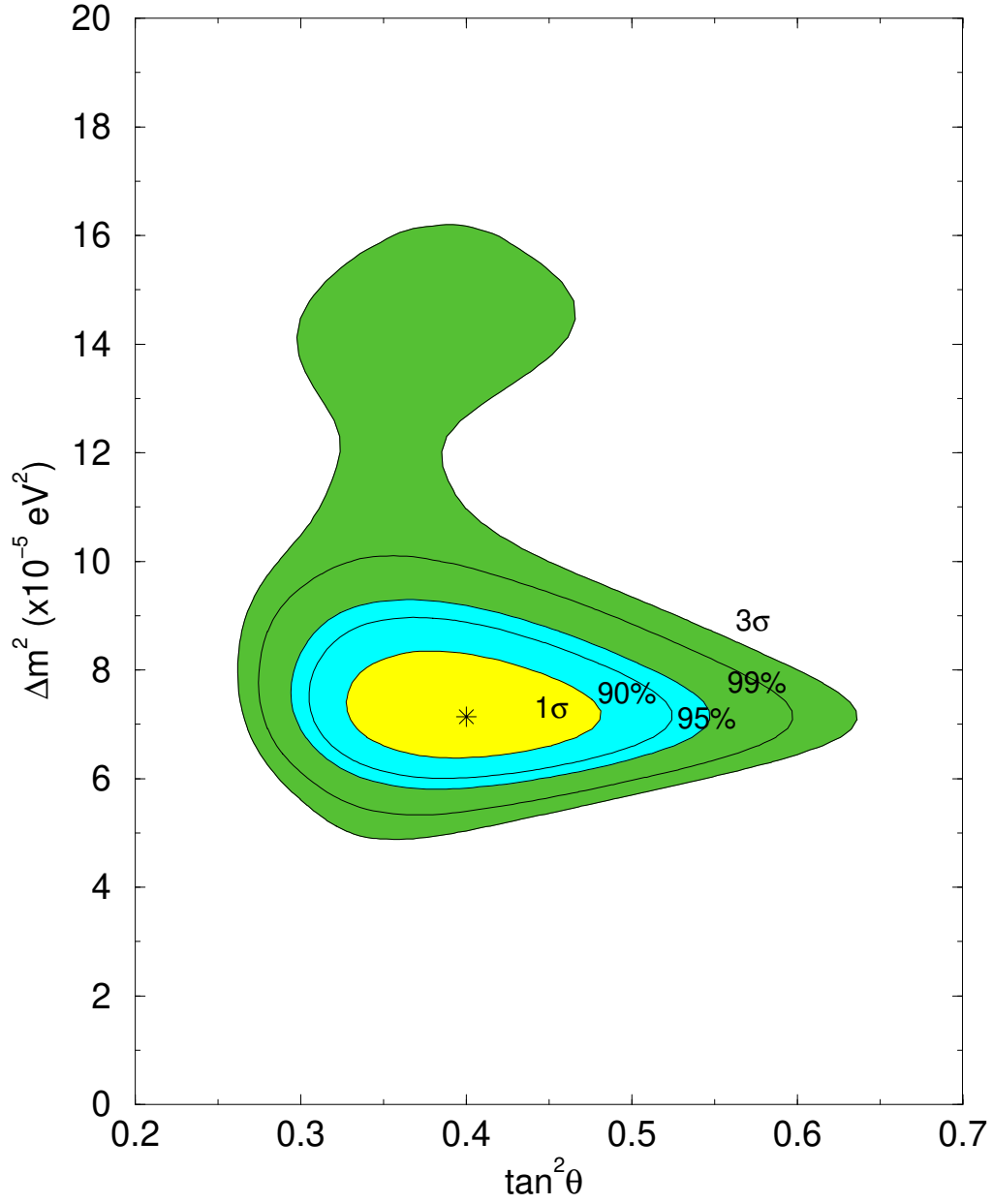


Figure 2: The allowed regions in  $\tan^2\theta$  -  $m^2$  plane, from a combined analysis of the solar neutrino data and the KamLAND spectrum at 1 , 90% , 95% , 99% and 3 C.L.. The boron neutrino flux is treated as free parameter. The best fit point is marked by star.

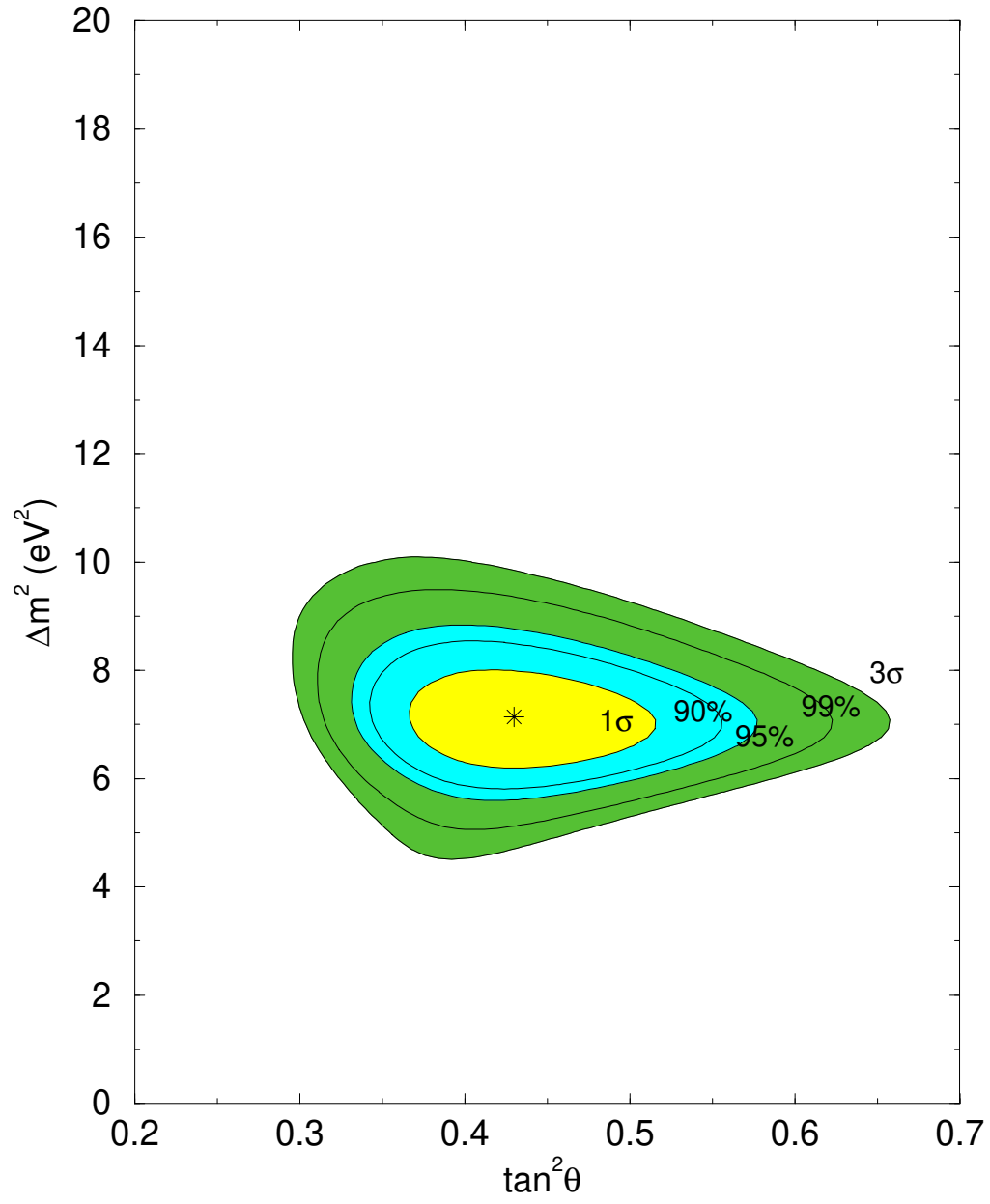


Figure 3: The same as in fig. 2 with the SSM predicted value of the boron neutrino flux.

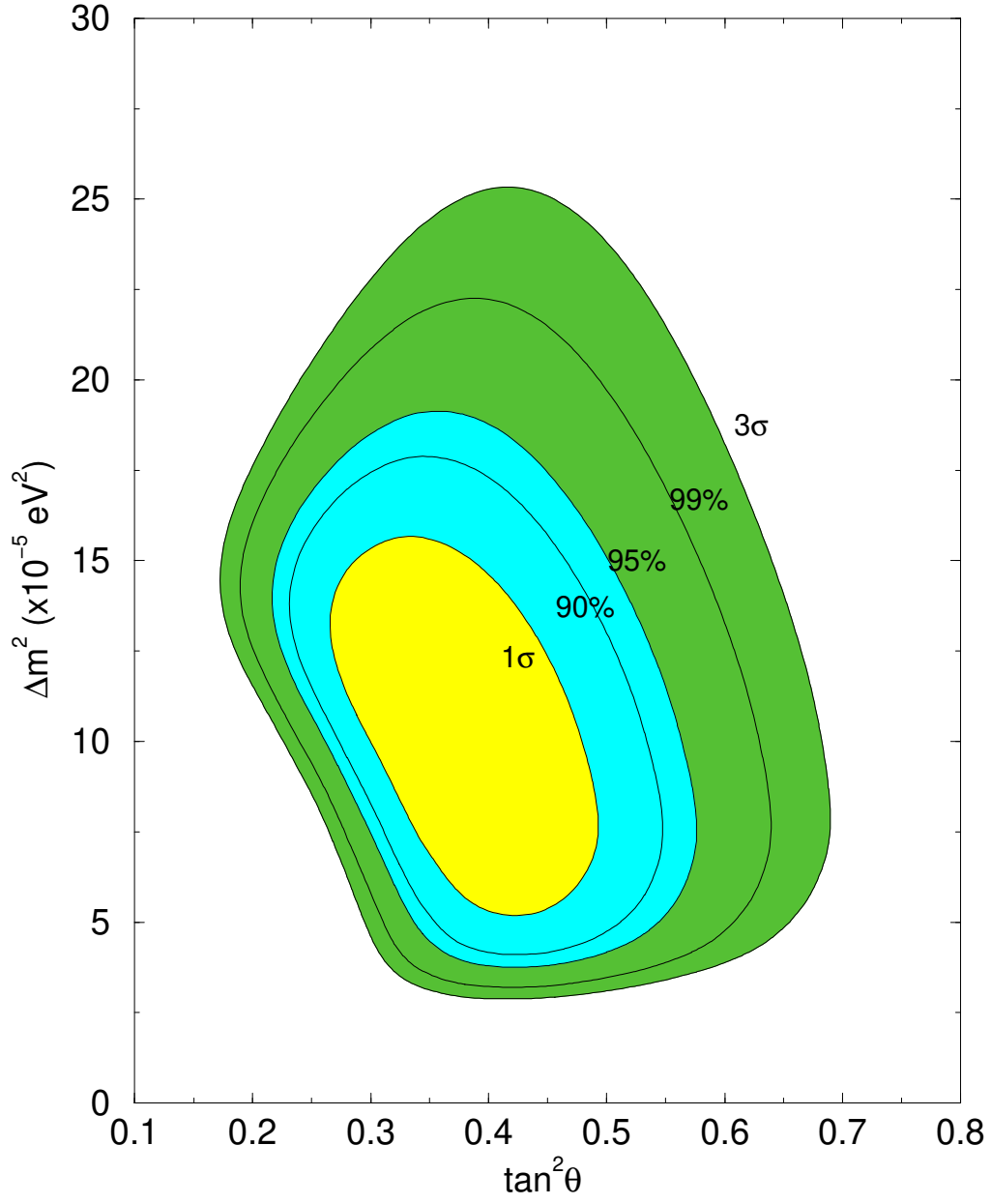


Figure 4: Three neutrino analysis with  $\sin^2 \theta_{13} = 0.067$ . The allowed regions in  $\tan^2 \theta$  vs  $\Delta m^2$  from a combined fit of the solar neutrino data at the 1  $\sigma$ , 90%, 95%, 99% and 3 C.L..

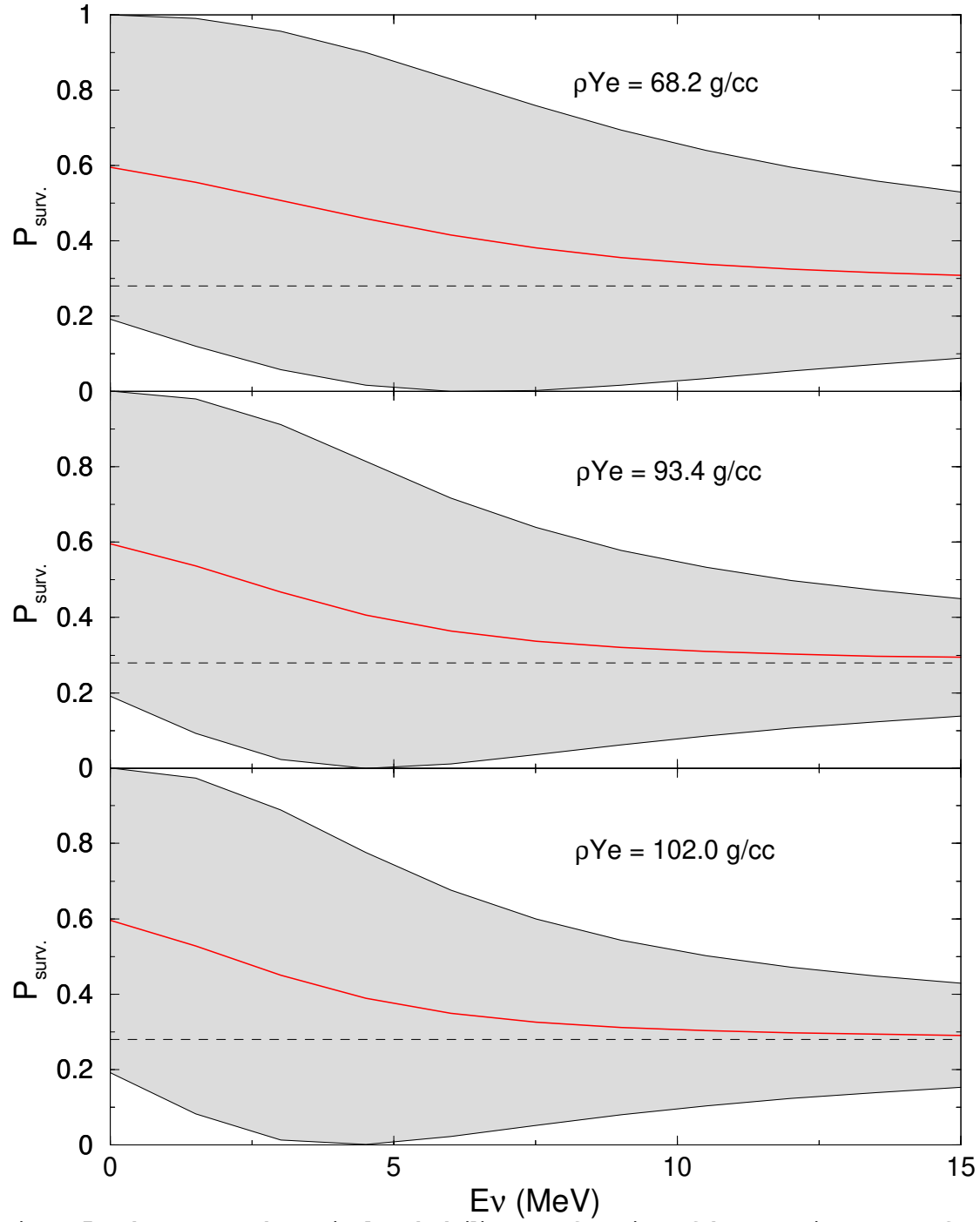


Figure 5: The averaged survival probability as a function of the neutrino energy for different production initial densities  $\rho_{Ye}$ . The oscillation strips (shadowed) show the depth of oscillations at the surface of the Sun. The non-oscillatory conversion probability  $P_{\text{non-osc}} = \sin^2$  is shown by the dashed line.



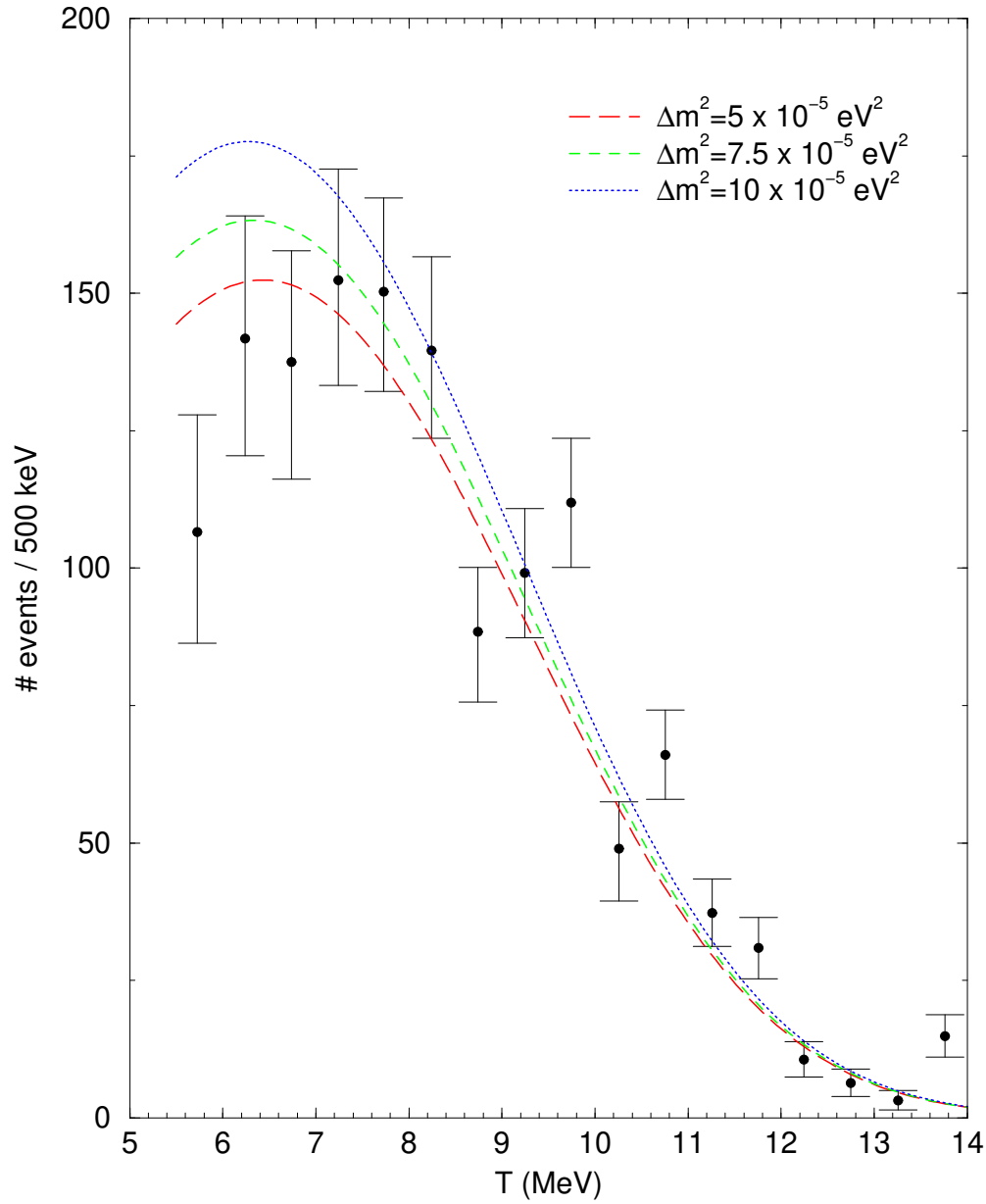


Figure 6: The energy spectrum of the CC reaction events. Shown is the distribution of events in the kinetic energy for different values of  $m^2$  and  $\tan^2 \theta = 0.39$ . We show also the SNO experimental points from the salt phase.

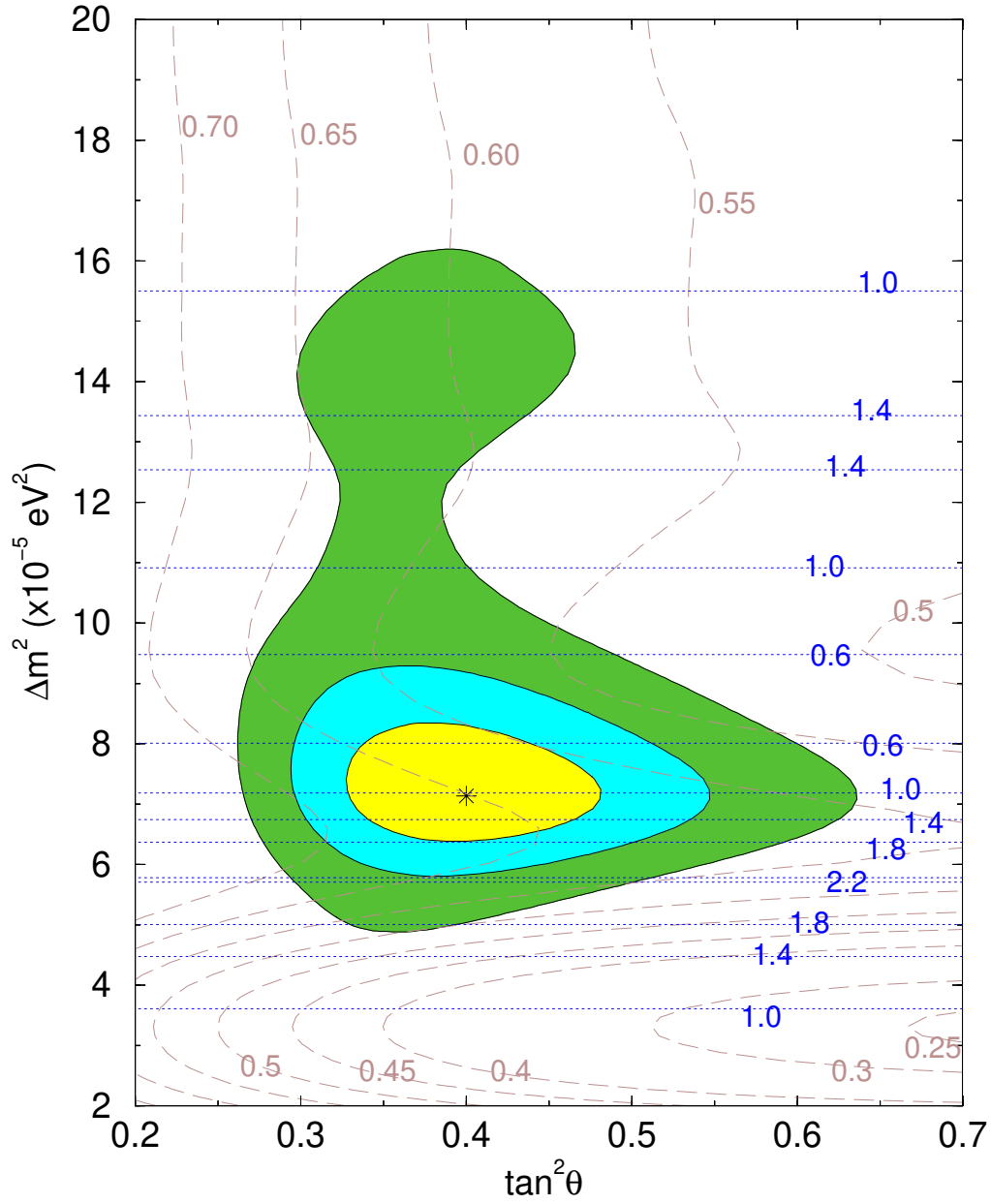


Figure 7: The contours of constant rate suppression,  $R_{KL}$  (dotted) and the spectrum shape parameter  $k$  (dashed) at KamLAND. We show also the allowed regions of the oscillation parameters from the combined fit of the solar neutrino data and the KamLAND spectrum. The best fit point is indicated by a star.

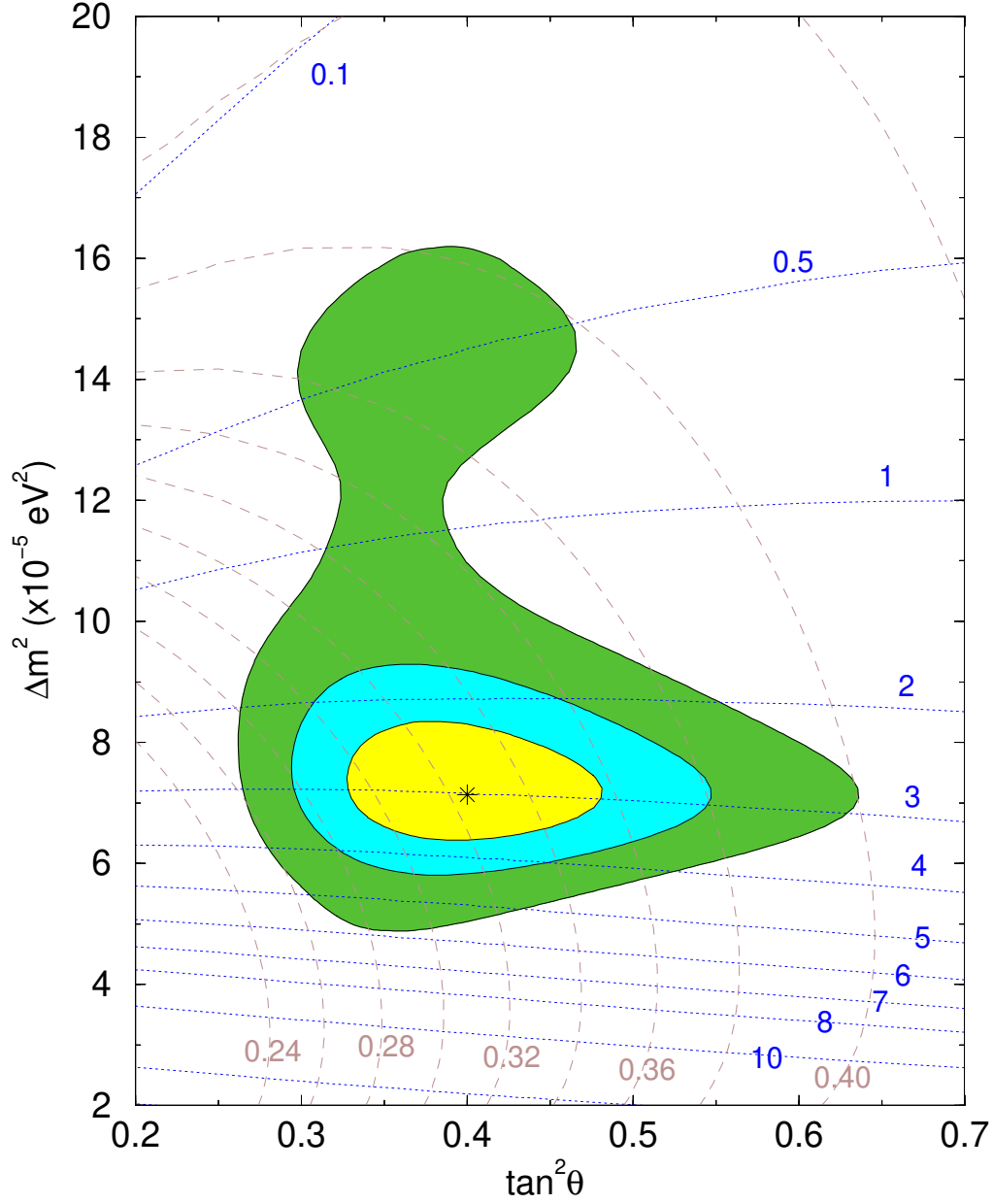


Figure 8: Predictions for the CC/NC ratio and the Day-Night asymmetry at SNO. The dashed lines are the lines of constant CC/NC ratio (numbers at the curves) and the dotted lines show the lines of constant  $A_{DN}^{SNO}$  (numbers at the curves in %). We show also the 1 and 3 allowed regions of the oscillation parameters from the combined fit of the solar neutrino data and the KamLAND spectrum. The best fit point is indicated by a star.

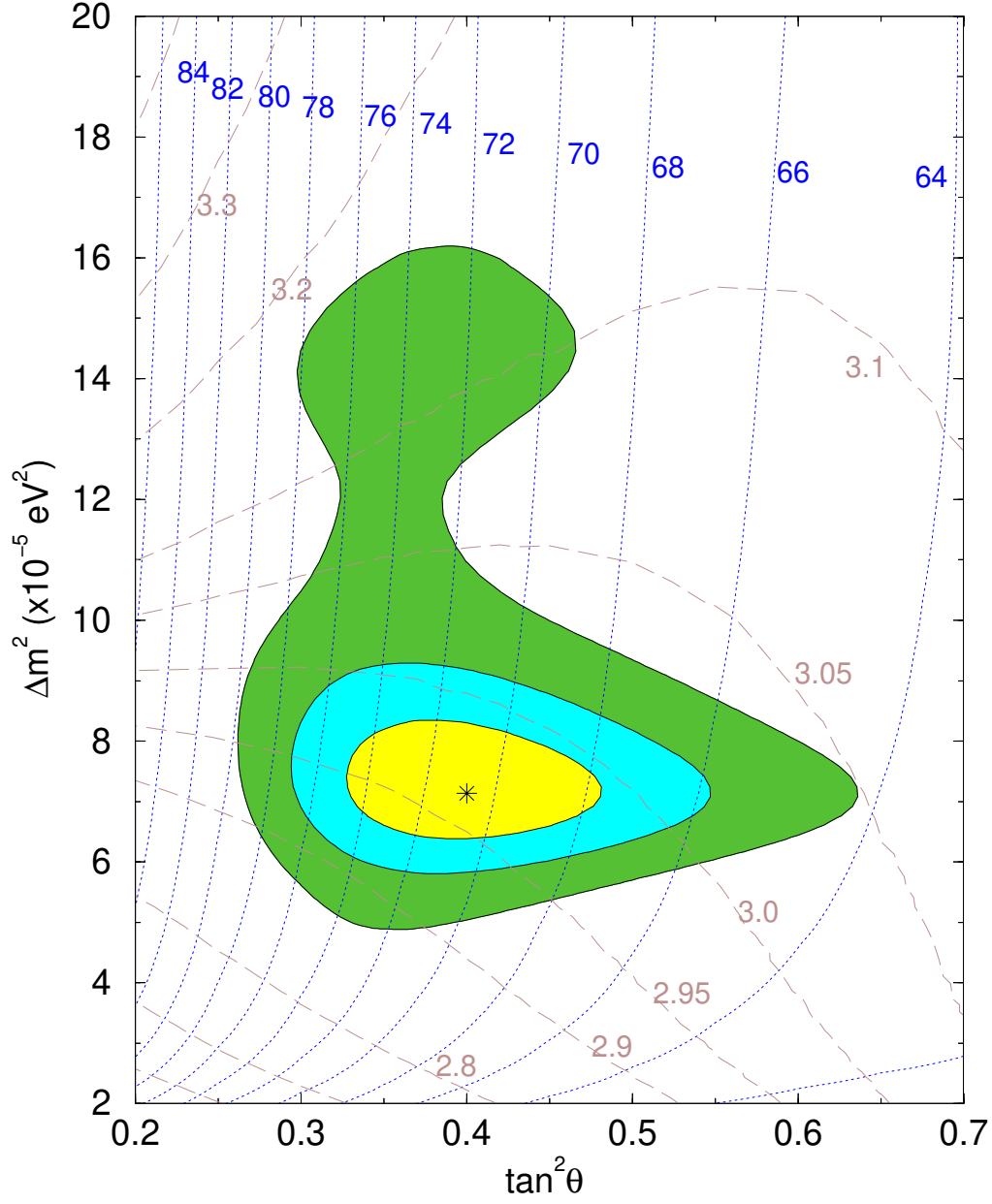


Figure 9: Predictions for the Germanium and Argon production rates. The dotted lines are the lines of constant Germanium production rate,  $Q_{\text{Ge}}$ , and the dashed lines show the lines of constant Argon production rate,  $Q_{\text{Ar}}$  (numbers at the curves in SNU), in the  $m^2 - \tan^2$  plane. We show also the allowed regions of the oscillation parameters from the combined fit of the solar neutrino data and the KamLAND spectrum. The best fit point is indicated by a star.